Atmospheric Research 297 (2024) 107122

Contents lists available at ScienceDirect

Atmospheric Research

journal homepage: www.elsevier.com/locate/atmosres

Artificial neural network-empowered projected future rainfall intensity-duration-frequency curves under changing climate

Bijoychandra S. Takhellambam [a,*], Puneet Srivastava [b], Jasmeet Lamba [a], Wenpeng Zhao [c], Hemendra Kumar [b], Di Tian [d], Roberto Molinari [e]

[a] Auburn University, Department of Biosystem Engineering, 350 Mell St, Auburn, AL 36849, USA
[b] University of Maryland, Agricultural Experiment Station, Symons Hall, 7998 Regents Drive, College Park, MD 20742, USA
[c] Tokyo Institute of Technology, Department of Transdisciplinary Science and Engineering, 152-8552 Tokyo, Japan
[d] Auburn University, Department of Crop, Soil and Environmental Sciences, 201 Funchess Hall, AL 36849, USA
[e] Auburn University, Department of Mathematics and Statistics, 201 Extension Hall, AL 36849, USA

ARTICLE INFO

Keywords:
ANN
Climate change
Stochastic
Rainfall disaggregation
Frequency analysis
IDF curves

ABSTRACT

With the increasing trend of greenhouse gases in the atmosphere, by 2052 the temperature is expected to rise by 1.5 °C from the Pre-industrial Period, affecting future extreme rainfall events. This necessitates quantifying extreme hydrologic events to plan and design hydrologic and hydraulic structures using rainfall Intensity-Duration-Frequency (IDF) curves to adapt to future climate scenarios. This study developed future projected IDF curves for the Southeast United States using disaggregated sub-hourly (15-, 30-, and 45-min) monthly maximum rainfall from 2030 to 2059 using five climate models under the Representative Concentration Pathway 8.5 scenario. A computationally efficient feed-forward back-propagation Artificial Neural Network (ANN)-based approach was found to be significantly superior for disaggregating rainfall to a stochastic model with an average Nash–Sutcliffe efficiency (NSE) ranging from 0.67 to 0.84. The study found that there is an increasing rate of future projected annual maximum rainfall intensities in the range of 7% to 36% with reference to the historical period. The spatial variation in future projected extreme rainfall depths showed that the Gulf-Atlantic coast and the Appalachian Mountains are expected to receive more extreme rainfalls.

1. Introduction

Extreme rainfall events pose a serious threat to the ecosystem and economy by amplifying both the magnitude and frequency of floods (Nerantzaki and Papalexiou, 2022; Rahaman et al., 2023; Zhao et al., 2023). Therefore, rainfall Intensity-Duration-Frequency (IDF) curves are used when planning and designing hydrologic and hydraulic structures (Mirhosseini et al., 2014; Yan et al., 2018). However, the existing structures for rainfall and floods designed are based on the stationarity of the IDF curves which give a probability of rainfall intensity in a given period, particularly National Oceanic and Atmospheric Administration Atlas 14 (Perica et al., 2013; Soltani et al., 2020; Sun et al., 2019; Zhao et al., 2022a, 2022b). In addition, the IDF curves are used in the design of erosion control structures, storm, and sewer drainage designs, and bridges (Amatya et al., 2021).

According to the IPCC (2018), by 2052 the temperature is expected to rise by 1.5 °C from the Pre-industrial Period with the current emission rate of greenhouse gases such as carbon dioxide, which eventually will affect future extreme rainfall events (Budhathoki et al., 2022; Takhellambam et al., 2023). The increase in temperature has resulted in higher water-holding capacity in the atmosphere, i.e., a 7% increase in water-holding capacity per degree Celsius of temperature (Easterling et al., 2017; Trenberth, 2011). The plausible effects include a change in rainfall amount, frequency, and intensities or probable maximum rainfalls (Cheng and AghaKouchak, 2014). Under these conditions, extreme rainfall events are expected to occur more frequently and with greater intensity in most parts of the world, with urban areas being the most vulnerable (Ghasemi Tousi et al., 2021). Therefore, to adapt or reduce the vulnerability of water management structures, future rainfall characteristics under the changing climate should be considered while developing IDF curves (Mirhosseini et al., 2014; Noor et al., 2022). For instance, the most critical component of cities' structures includes storm-water drainage and flood mitigation measured which are based on the IDF curves (Crévolin et al., 2023; Ghasemi Tousi et al., 2021).

* Corresponding author.
E-mail address: tzs0075@auburn.edu (B.S. Takhellambam).

https://doi.org/10.1016/j.atmosres.2023.107122
Received 2 June 2023; Received in revised form 22 October 2023; Accepted 19 November 2023
Available online 25 November 2023

Previous studies developed future projected IDF curves considering the nonstationary rainfall characteristics under changing climate (Cheng and AghaKouchak, 2014; Ganguli and Coulibaly, 2019; Ghasemi Tousi et al., 2021; Mirhosseini et al., 2013, 2014; Zhao et al., 2021). These studies employed Generalized Extreme Value (GEV) distribution for developing rainfall IDF curves owing to the better modeling of extreme rainfall events. Cheng and AghaKouchak (2014) reported an underestimation of extreme rainfall of up to 60% under the stationarity assumption compared to nonstationary conditions using five locations in the United States. Likewise, Ganguli and Coulibaly (2019) developed IDF curves under a nonstationary model over eight locations in the densely populated and major financial region of Southern Ontario, Canada. Ghasemi Tousi et al. (2021) updated the IDF curves for the city of Tucson, Arizona from 2020 to 2051 using eight global climate models. The findings showed a significant increase in the future extreme rainfall event which eventually needed to update IDF curves. In addition, the extreme values are found significantly affected with climate model selection and scenarios. For example, the stormwater culvert design could double the design size and significantly increase the cost based on the model selection and warming scenarios. Moreover, Noor et al. (2022) proposed IDF curves along with the uncertainty for the ungauged locations over Peninsular Malaysia. The results found that the shorter duration rainfall with a higher return period increased more than longer duration rainfall with a lower return period. Similarly, Mirhosseini et al. (2013) assessed future projected IDF curves using 15-min rainfall data in Alabama, United States. The 15-min rainfall was developed with 3-h rainfall data using a modified stochastic method of Socolofsky et al. (2001). This 15-min rainfall dataset was further used to develop IDF curves using the GEV distribution. The results demonstrated that less severe rainfall was anticipated for short-duration occurrences. However, the simulated rainfall intensities were under-predicted compared to the observed data. Mirhosseini et al. (2014) reported consistent results of underpredicted intensities. This was further improved by Mirhosseini et al. (2014) introducing a feedforward ANN approach. Thus, the IDF curves were further updated for future projected climate scenarios for Alabama using the GEV distribution and compared with the stochastically generated rainfall of Mirhosseini et al. (2013). The ANN method reported superior performances compared to the stochastic models in developing maximum rainfall depths. Further, rainfall events with less than a 2-h duration showed decreased intensities, and longer-duration storms with higher uncertainties (Mirhosseini et al., 2014).

Zhao et al. (2021) improved the ANN approach for rainfall disaggregation of Mirhosseini et al. (2014) through a computationally efficient and more accurate approach that was applied over two cities in southern Vietnam. The advantages include computationally efficient training data that used only extreme rainfall data points instead of the whole series and improving accuracy through the inclusion of previously simulated steps of rainfall. However, the Zhao et al. (2021) method provided a limited assessment of the hourly and multi-hourly scales.

In this study, we aimed to further extend the approach of Zhao et al. (2021) for disaggregating hourly to sub-hourly (15-, 30-, and 45-min) monthly maximum rainfall datasets. This is because sub-hourly rainfall aggregates offer greater intensities than hourly rainfall aggregates (Takhellambam et al., 2022a). McGehee and Srivastava (2018) reported that maximum rainfall intensity occurred within 15 min of a storm. So, aggregated datasets are underestimated due to the averaging of sub-hourly data. In addition, McGehee and Srivastava (2018); Takhellambam (2023); Takhellambam et al. (2022a,b) reported that the Southeast region of the United States has the greatest potential for change in rainfall characteristics under the changing climate. This necessitates updating the future IDF curves required for adequate hydrologic and hydraulic infrastructure designs, such as dams and culverts under the changing climate. We hypothesize that a feed forward and back propagation ANN model would perform better than the stochastic model in the disaggregation of hourly rainfall to sub-hourly (15-, 30-, and 45-min) rainfall datasets. Therefore, the objectives of this study were to: (1) generate sub-hourly (15-, 30-, and 45-min) monthly maximum rainfall datasets under the RCP 8.5 scenario using the feed forward and back propagation ANN model, and (2) develop the projected future rainfall IDF curves using the GEV distribution for the Southeast United States using improved sub-hourly rainfalls.

2. Material and methods

2.1. Study area and data

The average annual rainfall received in the Southeast United States (Fig. 1) is greater than the country's average of 856 mm. The annual rainfall ranges from 1000 to 1250 mm inland and can go as high as 1500 mm along the Gulf-Atlantic coastal areas (Ingram et al., 2013; Kumar et al., 2021, 2022a,b, 2023). The higher intensity rainfall is received on the Gulf-Atlantic coast and decreases inland. At the same time, the Appalachian Mountain region sees a greater rainfall intensity due to the orographic effect (Takhellambam et al., 2022a, 2023). The major factor for the distinctive climate in the region is due to the presence of both the Gulf of Mexico and the Atlantic Ocean (Ingram et al., 2013; Kunkel et al., 2013).

We obtained 44 years (1970–2013) of observed 15-min rainfall for 528 gauge data from the National Oceanic and Atmospheric Administration, DSI-3260, archived at the National Climatic Data Center (NOAA NCEI, 2014). McGehee et al. (2021) and Takhellambam et al. (2022a,b) recommended using the 20.11 screening method to check the quality of rainfall datasets and eventually found 187 stations that passed the screening method based on the precipitation deficit and spatial variations. Passing the 20.11 screening method requires a station to have a minimum of 20 years of complete observed precipitation for 11 or more months per year where a month must have atleast one observed rainfall event (McGehee and Srivastava, 2018; Takhellambam, 2023; Takhellambam et al., 2023). For the future projected 15-min rainfall data for the period 2030–59, we used five climate models for the future projected period (2030–59) of 15-min rainfall obtained from the North American Coordinated Regional Climate Downscaling Experiment (NA-CORDEX) under the RCP8.5 scenario. The five models included CANESM2_CANRCM4, HadGEM2-ES.WRF, GFDL-ESM2M.WRF, MPI-ESM-LR. RegCM4, and MPI-ESM-LR.WRF (Giorgi and Anyah, 2012; Scinocca et al., 2016; Skamarock et al., 2005). Hereinafter, we will refer to the climate model data as CANESM, HADGEM, GFDL, MPIREG, and MPIWRF, respectively. The Regional Climate Model-Global Climate Model (RCM-GCM) used GCM simulation of Coupled Model Intercomparison Project Phase 5 (CMIP5) archive. In addition, both temporal and spatial scales of these models are 1 h and 0.44^{o}, respectively (Mearns et al., 2017; Scinocca et al., 2016).

2.2. Bias-correction

The use of climate model data in hydrological-related studies has suffered from errors due to the simplified or limited representation at the regional scale (Takhellambam, 2023; Takhellambam et al., 2023). For instance, there are lower rainfall intensities with a large number of wet days which do not represent the observed rainfall intensities. To solve this problem, we used the quantile delta mapping method (Cannon et al., 2015; Takhellambam et al., 2023) suggested by Takhellambam et al. (2022a), whose performance were checked with annual average rainfall, intensity and wet-hour frequency. This method incorporates the non-stationarity of projected rainfall datasets which methods like quantile mapping failed to do so. The bias correction was carried out on a monthly scale to acquire intermittency of the rainfall while also preserving the rainfall characteristics.

$$\widehat{x}_{m,p.adjst.} = x_{m,p}\frac{F_o^{-1}\left(F_{m,p}\left(x_{m,p}\right)\right)}{F_{m,h}^{-1}\left(F_{m,p}\left(x_{m,p}\right)\right)} \quad (1)$$

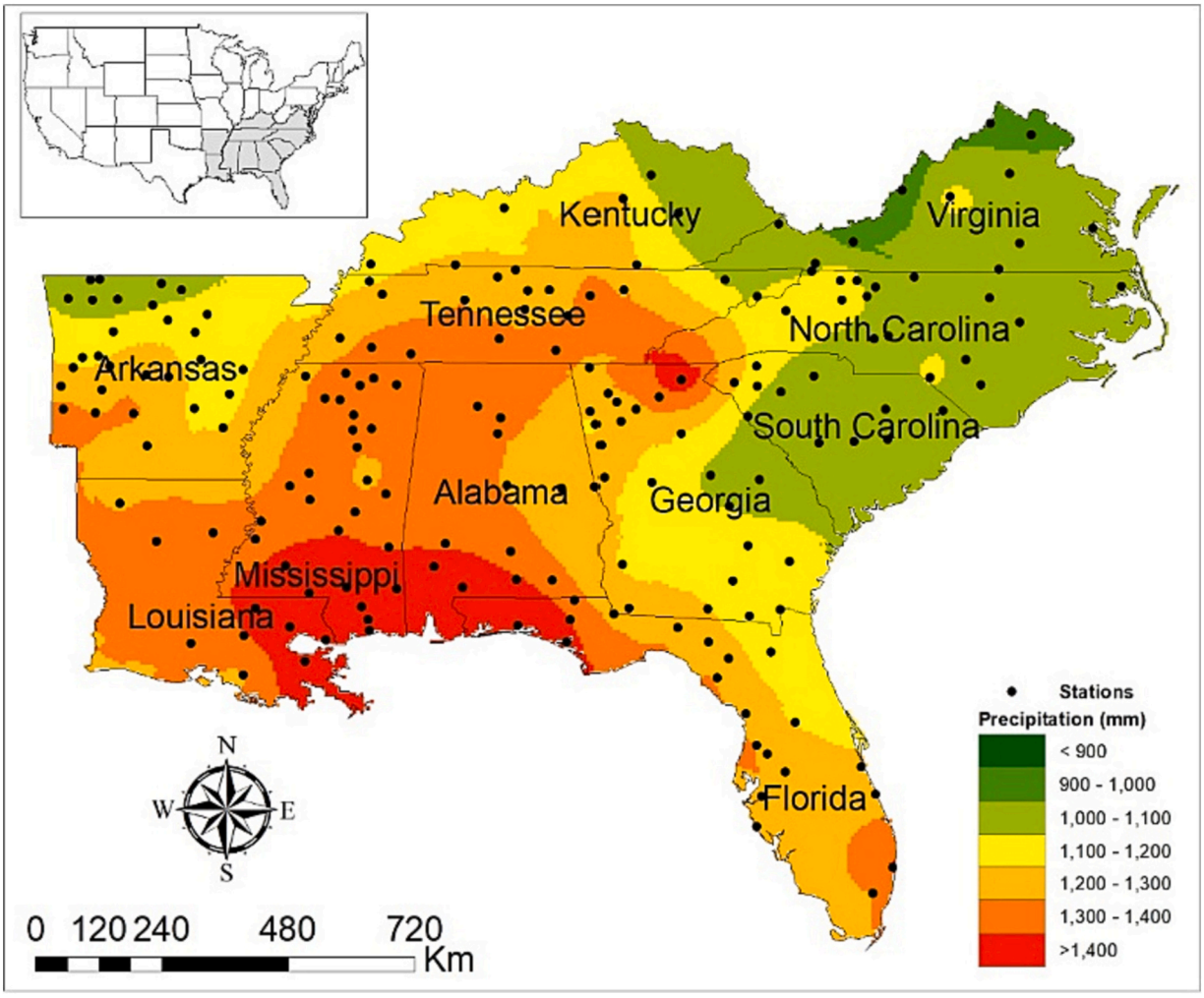

Fig. 1. Study area and location of observed 187 rainfall stations over the Southeast United States.

where x is the rainfall data, and F represents the cumulative probability distribution function for either the observed (o) or model-based (m) historical (h) and future projected (p) scenarios. From this onwards, we used the terms observed and historical to represent only observed datasets and climate model historical datasets, respectively.

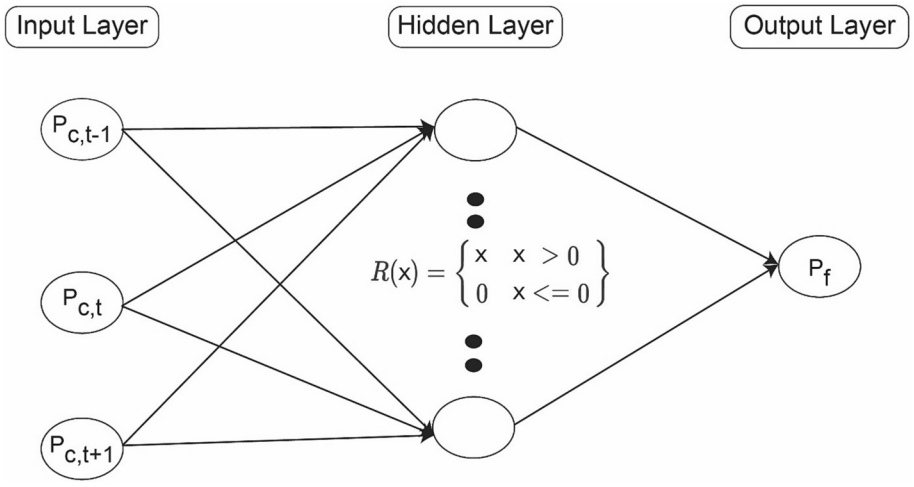

Fig. 2. An overview of the disaggregation of hourly (c) monthly maximum rainfall datasets to sub-hourly (f) monthly maximum rainfall datasets using activation of rectified linear unit function (R(x)). Here, P is the monthly maximum at a given time (t) step. t-1 and t + 1 are the preceding and subsequent hourly rainfall datasets, respectively.

2.3. Disaggregation of hourly rainfall to sub-hourly monthly maximum rainfall using ANN

The ANN model of Zhao et al. (2021), which was originally developed for disaggregating daily rainfall to sub-daily monthly maximum rainfall, was tested in this study for disaggregating hourly to sub-hourly (i.e., 15-, 30-, and 45-min) monthly maximum rainfall. This ANN model is a multi-layered perceptron neural network, where the output layer gives the sub-hourly monthly-maximum rainfall information based on the hourly information from the input layer. This has three layers of input, hidden, and output layers, with 20 neurons in the hidden layers which use the activation function of the rectified linear unit (ReLU). ReLU enables the model to learn more quickly and perform better (Brownlee, 2019). The loss function and optimizer are the mean squared error and root mean squared propagation (RMSprop), respectively.

We briefly introduce the ANN model below. We refer the readers to Zhao et al. (2021) for more details. To estimate the extreme rainfall amount at finer resolutions (sub-hour), the ANN model uses the concurrent, preceding, and succeeding rainfall at coarser resolutions (hourly) instead of the entire rainfall time series (Fig. 2). For instance, to obtain the extreme rainfall at the 15-min resolution, the ANN model extracts the total 1-h rainfall that occurs at the current time step as well as at the previous and subsequent time step (hourly scale). While developing the models, we used 70% and 30% of datasets for training and testing, respectively. Overall, we estimated (3 resolutions × 187) 561 models in our study area owing to the different rainfall generation mechanisms at different locations. For instance, the rainfall generation mechanisms in the Gulf-Atlantic coast and Appalachian Mountain are mainly due to the convective and orographic effects respectively.

2.4. Performance comparison in generating monthly maximum rainfall intensities

The assessment of the ANN's performance in disaggregating hourly to sub-hourly monthly maximum rainfall was conducted using the gauge observed rainfall data. We aggregated the observed 15-min rainfall into 1-h intervals. This rainfall data is then disaggregated to monthly maximum rainfall of 15-min using the feed-forward back-propagation ANN model. Similarly, we disaggregated the remaining temporal scales of 30- and 45-min rainfall datasets.

We compared the ANN-disaggregated monthly maximum 15-, 30-, and 45-min rainfall data with those of stochastically generated rainfall data by Takhellambam et al. (2022a). Since the stochastic data were available in continuous time series of rainfall at 15-min intervals, we also aggregated the 15-min scale to the scales of 30- and 45-min. Further, we extracted the monthly maximum rainfall from each of the 15-, 30-, and 45-min rainfall datasets. Thus, the performance of the monthly maximum rainfall of each scale using both the ANN and stochastically generated datasets was compared as discussed below.

More specifically, the statistical measures of Nash–Sutcliffe efficiency (NSE), Pearson correlation coefficient and Perccent bias (PBIAS) were used to assess the performance of rainfall disaggregation. These measures were computed for each station using the observed and disaggregated monthly maximum rainfall for the entire time series. These performance measures are defined below, starting with the NSE given by

$$NSE = 1 - \frac{\sum_{i=1}^{n}(o_i - m_i)^2}{\sum_{i=1}^{n}(o_i - \overline{o}_i)^2} \tag{2}$$

where, o = observed rainfall, $\overline{o}$ = average observed rainfall, m = model rainfall, and n = number of observations.

The Pearson correlation coefficient, in this setting, is defined as

$$r = \frac{\sum_{i=1}^{n}(o_i - \overline{o}_i)(m_i - \overline{m}_i)}{\sqrt{\left[\sum_{i=1}^{n}(o_i - \overline{o}_i)^2\right]}\sqrt{\left[\sum_{i=1}^{n}(m_i - \overline{m}_i)^2\right]}} \tag{3}$$

where $\overline{m}$ = average simulated rainfall.

The Percent bias is defined as

$$PBIAS = \frac{\sum_{i=1}^{n}(o_i - m_i)}{\sum_{i=1}^{n}(o_i)} \tag{4}$$

We hypothesized that the stochastic approach would outperform the ANN model in disaggregating the hourly to sub-hourly rainfall with the null hypothesis, H_0: the stochastic model performed equally with the ANN model. Subsequently, using a significance level of 5%, we used a one-sided paired Student *t*-test as well as a non-parametric Wilcoxon sign rank test (the latter to confirm that possible outliers do not impact the conclusion of the t-test).

2.5. Developing IDF curves

The Type-1 GEV distribution has been employed extensively in past studies owing to its simplicity and all useful moments are expressible with the two parameters of location and scale (Phien, 1987). Previous studies by Mirhosseini et al. (2013, 2014) reported that the GEV distribution well fitted developing rainfall IDF curves in the region, particularly the Gumbel distribution. The GEV probability distribution consists of three limiting forms i.e., Gumbel ($\xi \to 0$), Frechet ($\xi > 0$), and Weibull ($\xi < 0$) (Coles, 2001) and is defined as follows.

$$G(\mathrm{x}) = exp\left\{-\left[1 + \xi\left(\frac{\mathrm{x} - \mu}{\sigma}\right)\right]^{-1/\xi}\right\} \text{ for } x : 1 + \xi\left(\frac{\mathrm{x} - \mu}{\sigma}\right) > 0 \tag{5}$$

where x is the rainfall intensity. μ, σ, and ξ are location, scale, and shape parameters respectively. The Gumbel distribution with $\xi \to 0$ is defined as

$$G(\mathrm{x}) = exp\left[-exp\left\{-\left(\frac{\mathrm{x} - \mu}{\sigma}\right)\right\}\right] \text{ for } x : 1 + \xi\left(\frac{\mathrm{x} - \mu}{\sigma}\right) > 0 \tag{6}$$

In addition, the parameter estimation is performed using maximum likelihood estimation since, if the model is correctly specified, it has optimal statistical properties compared to other methods such as the method of moments (Mahdi and Cenac, 2005). The Kolmogorov-Smirnov (KS) test is used to test the goodness-of-fit at a significance level of 5% assuming the parameters are known (Delignette-Muller and Dutang, 2015), keeping in mind that, this test could be conservative i.e., not reject H_0 when it should (Lilliefors, 1967). The following procedure was used to obtain the IDF curves.

1) Obtain the annual maximum series of rainfall for a given duration (T) of 15-, 30-, and 45-min.
2) Evaluate the rainfall depth, X_T for a given return period (2-, 5-, 25-, 50-, and 100-year) for the Gumbel distribution which is given by.

$$X_T = \overline{x} + K_T S \tag{7}$$

where, $\overline{x}$, K_T, and S are mean, frequency factor, and standard deviation, respectively.

$$K_T = -\frac{\sqrt{6}}{\pi}\left[0.5772 + ln\left(ln\left(\frac{T}{T-1}\right)\right)\right] \tag{8}$$

3) The rainfall depths are plotted for each duration for different return periods.

3. Results and discussion

The performance of the ANN in disaggregating 1-h rainfall to monthly maximum 15-, 30-, and 45-min rainfall is reported below. The monthly maximum rainfall intensities are then compared between the stochastic and the ANN models. Finally, using ANN, the results of the generated future IDF curves are presented alongside historical and projected future scenarios.

3.1. Performance of bias correction and ANN for rainfall disaggregation

Bias correction improved the output of the climate models, especially the frequencies of wet days, annual average rainfall amount, and rainfall intensity. A detailed explanation for the performance of bias correction of hourly rainfall is given in Takhellambam et al. (2022a). The performance of disaggregated rainfall using the ANN approach was assessed by employing the Pearson correlation coefficient (r) and the Root mean square error (RMSE) in both training and test data for the generation of 15-, 30-, and 45-min monthly maximum rainfall and reported for the 187 rainfall stations. The RMSE values are reported with normalization of both training and testing datasets that removes the median and scales using the interquartile range i.e., RMSE has no unit. The minimum and maximum r values of the training datasets were 0.75 and 0.90, respectively (Fig. 3). On the other hand, as expected, the r values on the test datasets were found to be lower than those of the training datasets, with minimum and maximum of 0.62 and 0.88, respectively. The average r value for disaggregating to 15-min was found to be 0.84 and 0.77 for training and test data, respectively. Likewise, the RMSE value has an average value of 0.37 and 0.48 for training and test data, respectively.

The r value when disaggregating to 30-min rainfall was found to have an average value of 0.92 in training and 0.90 in test data. The range of values during training and testing were (0.89, 0.96) and (0.8, 0.97), respectively. Furthermore, we found that the RMSE value in both training and test data ranges from 0.21 to 0.4, and 0.22 to 0.58, respectively (Fig. 3). Similarly, the disaggregation to 45-min rainfall was found to have an average r value of 0.95 and 0.93 in training and test data. The r values during training and test range from (0.92, 0.98) and (0.87, 0.98, respectively. RMSE values showed ranges of (0.16, 0.36) and (0.19, 0.48) for training and test data, respectively. These results are in line with the results of Zhao et al. (2021). As expected, the performance of the ANN is satisfactory with $r > 0.60$ in disaggregating to the monthly maximum sub-hourly scale using the hourly rainfall datasets (Mirhosseini et al., 2014). Moreover, we found a better performance for longer periods of 30- and 45-min of rainfall datasets compared to the 15-min disaggregating of monthly maximum rainfall data. This better performance of the ANN with longer durations for disaggregating rainfall datasets is consistent with Mirhosseini et al. (2014). One of the main reasons for this is mainly due to the fact that hourly rainfall provides less information as the gaps in resolution become larger (Zhao et al., 2021), i.e., there is the smoothing of rainfall intensities while aggregating the 15-min to 30- and 45-min rainfall datasets (Op de Hipt et al., 2018).

We further compared the performance of the ANN in disaggregating hourly rainfall to the sub-hourly monthly maximum with a recently developed stochastically-generated 15-min rainfall dataset of Takhellambam et al. (2022a). We compared the stochastic and ANN methods in generating the monthly maximum rainfall using the 1-h data (Figs. 4 and 5). The quantile-quantile plot shows that the performance of the stochastic method is closely related to the observed rainfall for smaller rainfall depths (the solid line represents the perfect model). However, as the rainfall depth increases, the stochastic model shows an increase in the variance in all the temporal scales of 15-, 30-, and 45-min. Takhellambam et al. (2022a) concluded that the stochastic method underestimated the rainfall intensities compared to the observed datasets with an average NSE and r ranging from 0.48 to 0.8 and 0.78 to 0.9, respectively (Fig. 5).

The quantile-quantile plot of the ANN method shows a better performance with smaller variance than the stochastic method (Fig. 4), especially with higher rainfall intensities. The average NSE, r and PBIAS values were found in the range of 0.67 to 0.85,0.83 to 0.92, and 0.05 to 0.07 respectively (Fig. 5). This indicated that the ANN has a satisfactory performance when generating monthly maximum rainfall of 15-, 30-, and 45-min from 1-h data since its NSE is >0.6 (Mirhosseini et al., 2014).

Moreover, we found the null hypothesis of better performance of stochastic approach than the ANN model in disaggregating hourly data to a monthly maximum of sub-hourly rainfall data is rejected (p-value~0) using one-sided Student t-test and Wilcoxon sign rank test,

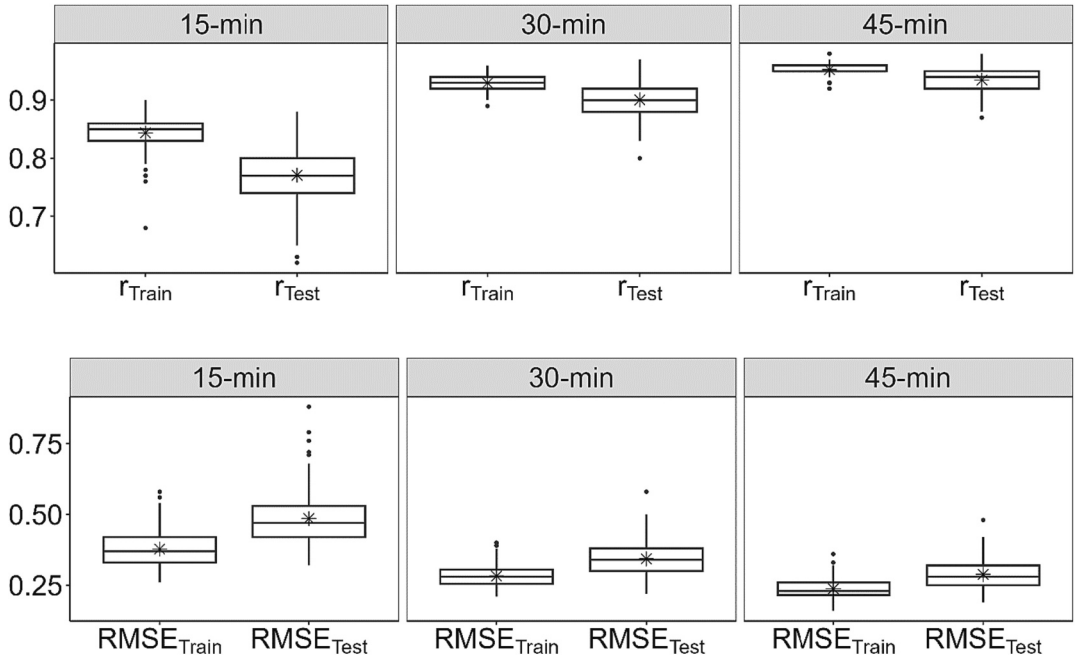

Fig. 3. Boxplots showing the performance comparison of the ANN model for disaggregating hourly to sub-hourly monthly maximum rainfall data during training (denoted by test) and testing (denoted by train) for 187 stations. Asterisk denotes the average value of coefficient of correlation and RMSE value.

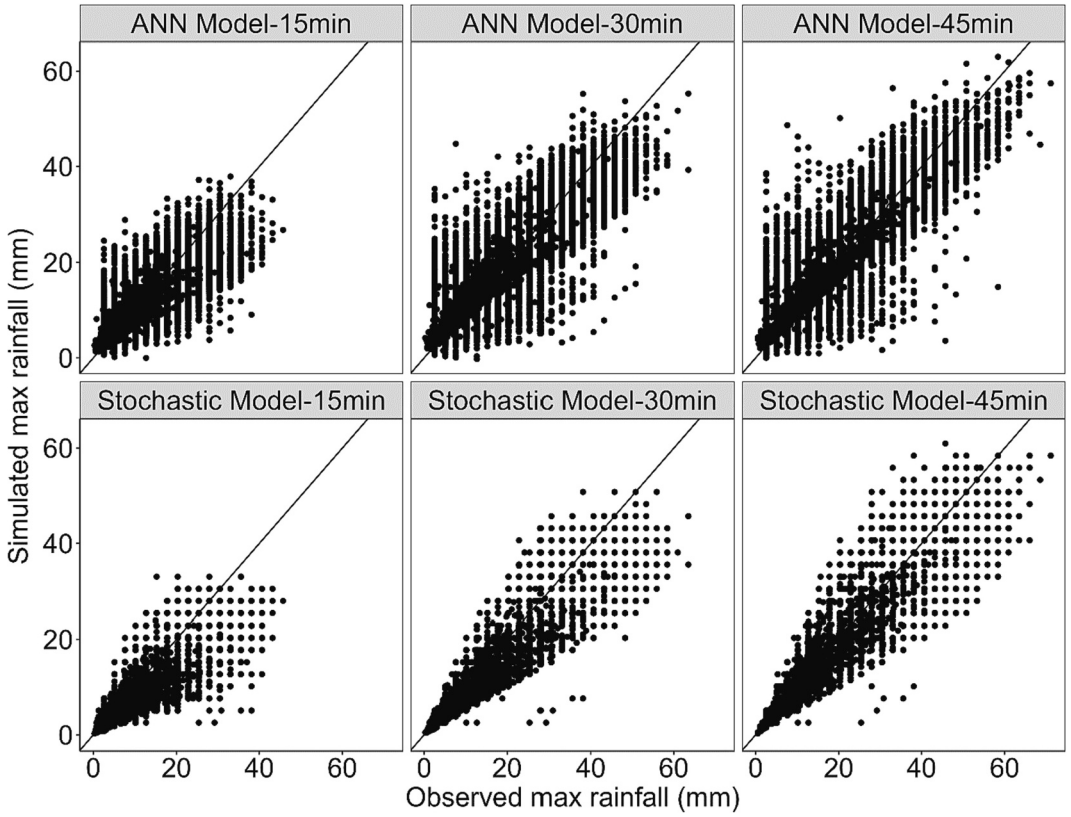

Fig. 4. Quantile-quantile plot for comparing ANN and stochastic model in temporal downscaling of hourly to sub-hourly monthly maximum of 15-, 30-, and 45-min rainfall for all 187 stations.

favoring the alternate hypothesis (at a 5% significance level). Therefore, we conclude that the ANN model's performance is superior compared to the stochastic model in generating 15-, 30-, and 45-min monthly maximum rainfall from 1-h rainfall. Previous studies also found similar results of superior performance by the ANN model over other disaggregation methods, especially compared to the stochastic method (Mirhosseini et al., 2014; Zhao et al., 2021). This is because neural networks can perform better in approximating complex relationships. The unique structure of the ANN, which connects each hidden layer to the output nodes provides a better approximation of complex non-linear relationships with no major distributional assumptions (Dibike and Coulibaly, 2006; Mirhosseini et al., 2014).

3.2. Rainfall intensity duration frequency curves

The future projected rainfall IDF curves were developed using durations of 15-, 30-, and 45-min with return periods of 2-, 5-, 10-, 25-, 50-, and 100-year using five climate models under the RCP8.5 scenario for the Southeast United States. We used kriging interpolation to generate a spatial variation of extreme rainfalls that provides an understanding and identification of extreme rainfall areas. This resulted in 90 different maps (5 RCMs per 6 Return Periods per 3 Durations). For brevity, we provide maps for all durations with return periods of 25-, 50-, and 100-year for the CANESM model (Fig. 6). The remaining models are presented in the supplementary file (Supplementary Figs. S1–S4). Fig. 6 shows the spatial variations of future projected annual maximum rainfall intensities of 15-, 30-, and 45-min with a return period of 25-, 50-, and 100-year using the CANESM model. This provides information on rainfall magnitude and recurrence of extreme rainfall intensities based on frequency analysis (Ragno et al., 2018).

The maximum annual rainfall intensity using the duration of 15-min under the CANESM model was found to range from 30 to 234 mm/h under 2-, 5-, 10-, 25-, 50-, and 100- year return periods. Likewise, the maximum annual rainfall intensity for the remaining duration of 30-, and 45-min ranged from 22 to 193 mm/h and 15 to 148 mm/h, respectively. We observed (Fig. 6) that the extreme rainfall intensities of annual maximum of 15-, 30-, and 45-min with the return period of 25-, 50-, and 100-year are mostly found in both the Gulf-Atlantic coast and the Appalachian Mountains. The remaining climate models also found results consistent with this (see Supplementary Figs. S1–S4). This demonstrates the similar higher and lower trend of both annual average and maximum rainfall intensities over the region (Takhellambam et al., 2023). Among these models, the MPIREG model found greater maximum rainfall intensities. The remaining models of HADGEM, GFDL, MPIREG, and MPIWRF for all durations showed maximum rainfall intensities ranging from 20 to 227 mm/h, 16 to 168 mm/h, 16 to 259 mm/h, and 16 to 239 mm/h, respectively, in given return periods of 2-, 5-, 10-, 25-, 50-, and 100-year. The differences among these models, among others, are due to the different mechanisms for generating rainfall (Mirhosseini et al., 2014). These multiple models enable us to quantify the ranges of maximum rainfall intensities.

Convective rainfalls cause more rain to fall along the Gulf and Atlantic coasts. This is due to the warm, humid, and subtropical air from the coastal areas that result in a greater number of intense rainfall events, especially from May to September (Kim et al., 2020; Perica et al., 2013). This further brings intense rainfall inland and provides greater rainfall in the flat regions (Takhellambam et al., 2022a). Moreover, the Appalachian Mountains receive higher rainfalls due to the orographic effect (Takhellambam et al., 2022a). In addition, the 15-min datasets have greater intensities as compared to the aggregated datasets of 30 and 45-min which is due to the smoothing of rainfall intensities. For instance, the peak rainfall intensity of smaller temporal scales is averaged over the scale of 30-min or 45-min resulting in decreased intensity.

For better discussion, we selected five rain-gauge stations across the region (Table 1), three of which are in urban areas, namely Venice, New Orleans Audubon, and Mullins, while the other two are in sparsely

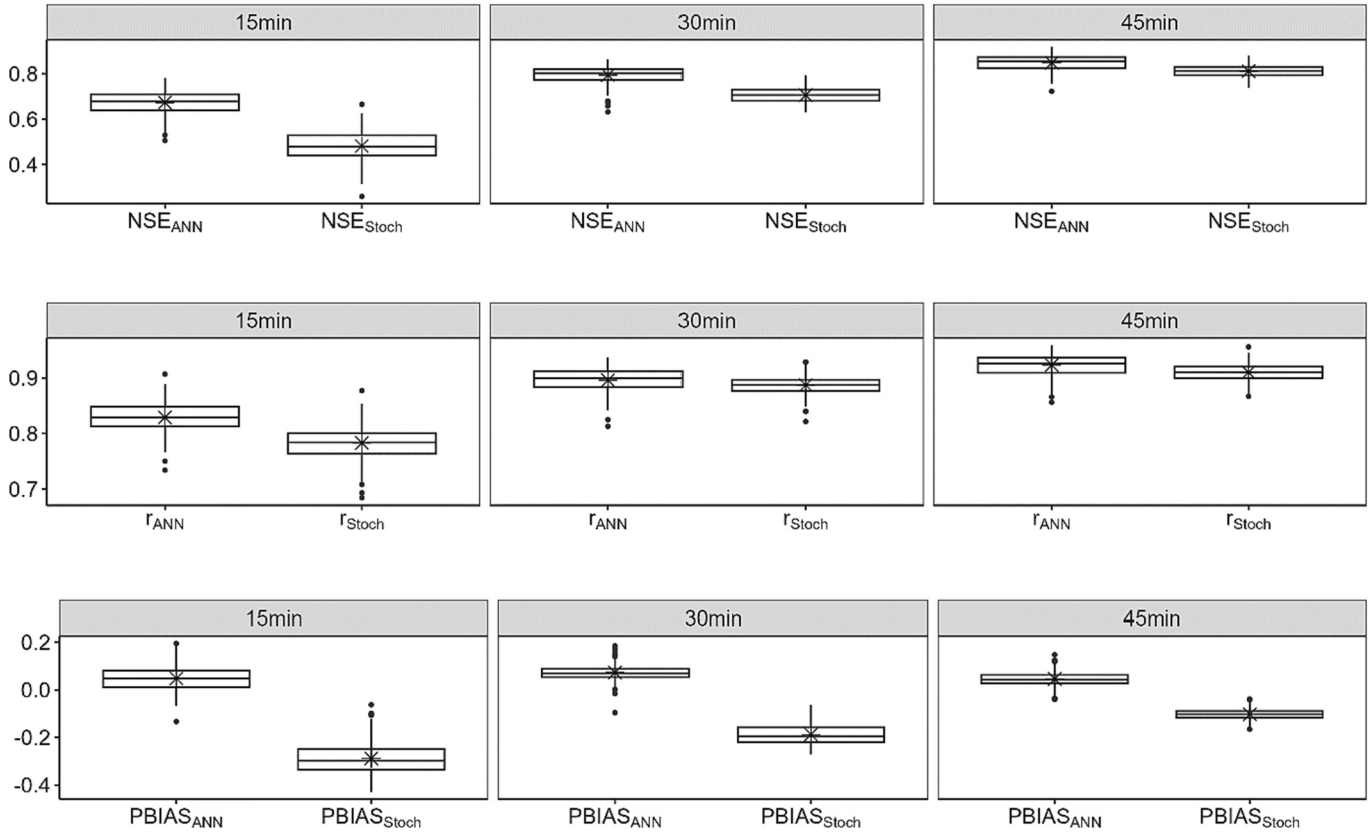

Fig. 5. Boxplots showing the statistical comparison between ANN (denoted by ANN) and stochastic (denoted by Stoch) model for disaggregating hourly to sub-hourly monthly maximum rainfall for 187 stations. The asterisk denotes the average value of the coefficient of correlation, NSE and PBIAS value.

inhabited areas which also considers the regions where convective and orographic rainfalls in the region. Table 2 shows the comparison of annual maximum rainfall intensities of 15- and 30-min duration with return periods of 2-, 5-, 10-, 25-, 50-, and 100-year between our study using the observed data (hereinafter referred to as OBS in Table 2) and findings of NOAA's National Weather Service (hereinafter referred to NWS) Atlas 14, volume 9, version 2 (Perica et al., 2013). The NWS findings of annual maximum rainfall intensities of 15-min with a 2-year return period show a range from 82 to 120 mm/h. Moreover, the extreme rainfall intensity of 100-year shows a minimum and maximum of 162 mm/h and 238 mm/h respectively. Our study using the observed annual maximum rainfall intensities of 15-min ranged from 65 to 103 mm/h with a recurring period of 2-year. In addition, a 100-year return period of 15-min rainfall intensities shows in the range of 122 to 168 mm/h, respectively. Furthermore, the NWS's annual maximum rainfall intensities of 30-min in all return periods ranges from 60 to 187 mm/h, while our study shows rainfall intensities was in the range of 43 to 125 mm/h.

All the annual maximum rainfall intensities in our study have been underpredicted compared to the NWS findings that range from 10% to 41%. One of the primary reasons for the disparity in rainfall depths is the parameter estimation approach used for the Gumbel distribution which then allows to delivery of the IDF curves. For example, NWS used L-moment-based regional frequency analysis, whereas our study used maximum likelihood estimation.

For the same locations discussed above (Table 1), we compared annual maximum rainfall intensities between the future projected and historical scenarios. We combine all five climate model outputs as a single ensemble. This allows the combining of various sources of information from different models to minimize the uncertainty associated with each model. We further show the ensemble annual maximum rainfall intensities (Fig. 7) of 15-, 30-, and 45-min with return intervals of 2-, 5-, 10-, 25-, 50-, and 100-year between the historical and future periods using the ANN located at Unicoi State Park (34.72°N, −83.72°W). The shaded area represents both future and historical IDF curves with 95% confidence intervals. We refer the reader to the supplementary file (Supplementary Figs. S5–S8) for the remaining four locations of Huntsville 1 SSW, Venice, New Orleans Audubon, and Mullins. We found that the historical annual maximum rainfall intensities at Unicoi State Park ranges from 26 to 54 mm/h with a return period of 2-year. The rainfall intensities increase with larger recurring intervals, with the greatest value in 100-year that ranges from 49 to 107 mm/h. Moreover, we found that the annual maximum rainfall intensities under future scenarios increased compared to the historical period for each duration and recurring interval. The rate of increase in the future rainfall intensity ranges from 16% to 29% (Table 3).

Similarly, the historical annual maximum rainfall intensities of 15-, 30-, and 45-min with a return period of 2-, 5-, 10-, 25-, 50-, and 100-year in the remaining locations has a minimum and maximum of 25 to 134 mm/h. Future scenarios show increasing rainfall intensities in all of the locations as compared to the historical period ranging from 7% to 36%. Overall, the minimum and maximum rainfall intensities under future scenarios were found in the range of 28 to 169 mm/h. The aforementioned findings indicate that the future projected extreme rainfall depths are significantly increased from the historical scenario for the Southeast United States.

3.3. Uncertainty in the IDF curves

Large uncertainties are associated with developed IDF curves owing to the variety of factors in both observed and model datasets. Most of the observed rainfall measurement methods and products are associated with inaccurate measurements due to the loss of rainfall characteristics i.e., amount, frequency, and intensity. This includes human error,

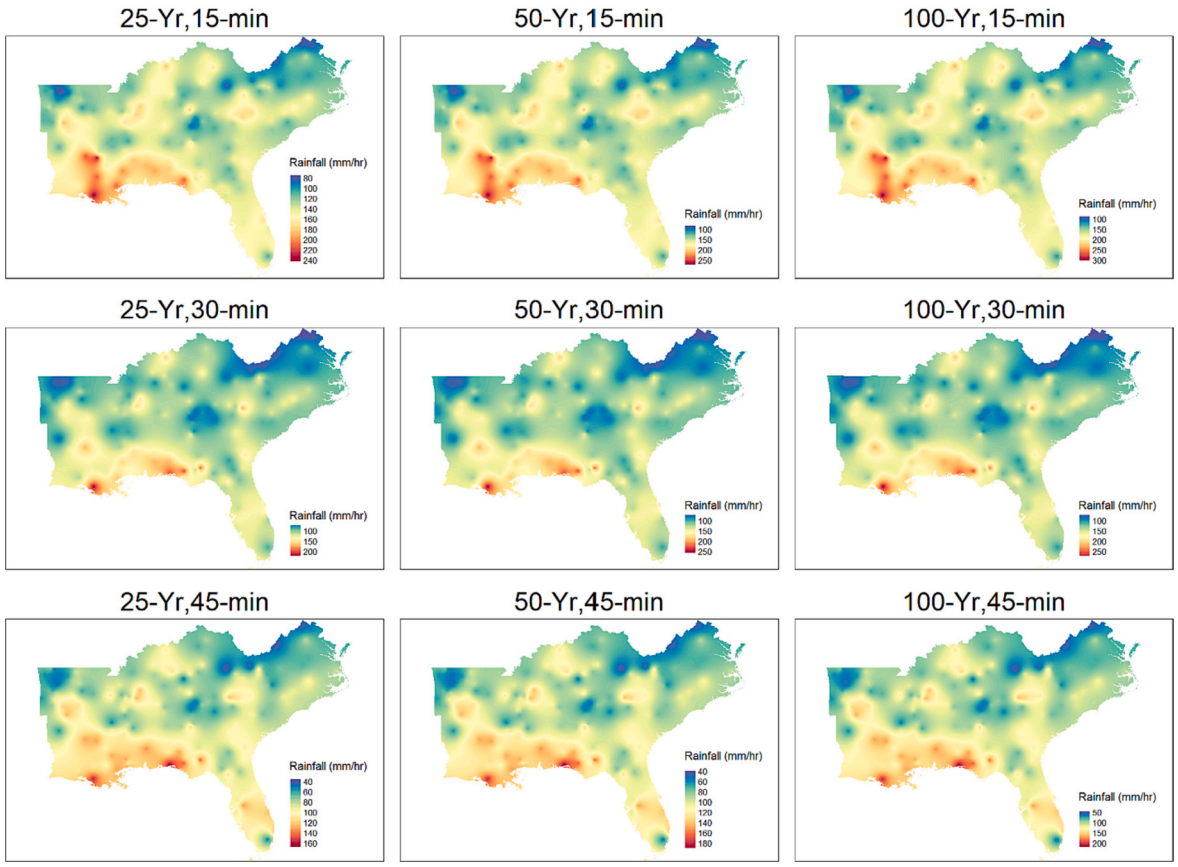

Fig. 6. Map showing the spatial variation of annual maximum rainfall intensities for 15-, 30-, and 45-min with a return period of 25-, 50-, and 100-year under CANESM.

Table 1
Descriptions of selected locations for the assessment of IDF curves.

Sl. No.	Name of station	Latitude (°N)	Longitude (°W)	Elevation (feet)
1	Huntsville 1 SSW	36.07	−93.75	1783
2	Venice	27.1	−82.44	8
3	Unicoi State Park New Orleans	34.72	−83.72	1594
4	Audubon	29.92	−90.13	20
5	Mullins	34.19	−79.25	110

measurement thresholds, evaporation, and wind effects. However, it is challenging to verify these errors in our rainfall dataset of observed events (Zhao et al., 2021).

According to Mirhosseini et al. (2013), uncertainty may result from the physical parametrization of climate models, such as the development of the rainfall process in various models, or the varied boundary conditions of climate projections. In addition, the typical climate model bias is a consequence of many wet days with low rainfall intensities (Takhellambam et al., 2023). Therefore, we are using multiple climate models to capture the various uncertainties associated with different climate models. The uncertainty associated with each model for future projected rainfall IDF curves was quantified with mean rainfall values along with standard deviation using all stations (Fig. 8). Under the CANESM model, the mean rainfall intensities and standard deviation range from 34 to 130 mm/h and 8 to 28 mm/h, respectively. Likewise, the remaining models show both mean rainfall intensity and standard deviation in the range of 34 to 135 mm/h and 7 to 28 mm/h,

Table 2
Comparison of annual maximum rainfall intensities (in mm/h) of 15- and 30-min duration with return periods of 2-, 5-, 10-, 25-, 50-, and 100-year between our study using the observed data (denoted by OBS) observed data and findings of NOAA's National Weather Service (denoted by NWS).

Station	Dur	Return period (years)											
		2		5		10		25		50		100	
		NWS	OBS	NWS	OBS	NWS	OBS	NWS	OBS	NWS	OBS	NWS	OBS
	15-min	82	65	98	80	112	90	132	103	147	113	162	122
Huntsville 1 SSW	30-min	60	43	73	50	83	56	97	62	109	67	120	71
	15-min	120	98	142	115	159	125	182	139	200	149	216	158
Venice	30-min	90	64	107	77	120	85	137	96	150	104	163	112
	15-min	90	69	108	85	124	96	147	109	166	119	186	129
Unicoi State Park	30-min	64	44	77	54	89	61	105	70	119	76	133	82
	15-min	114	103	138	120	159	132	189	147	213	157	238	168
New Orleans Audubon	30-min	88	69	107	84	124	94	148	107	167	116	187	125
	15-min	109	76	128	94	143	106	161	121	175	132	188	144
Mullins	30-min	75	48	91	60	104	68	119	77	132	84	144	91

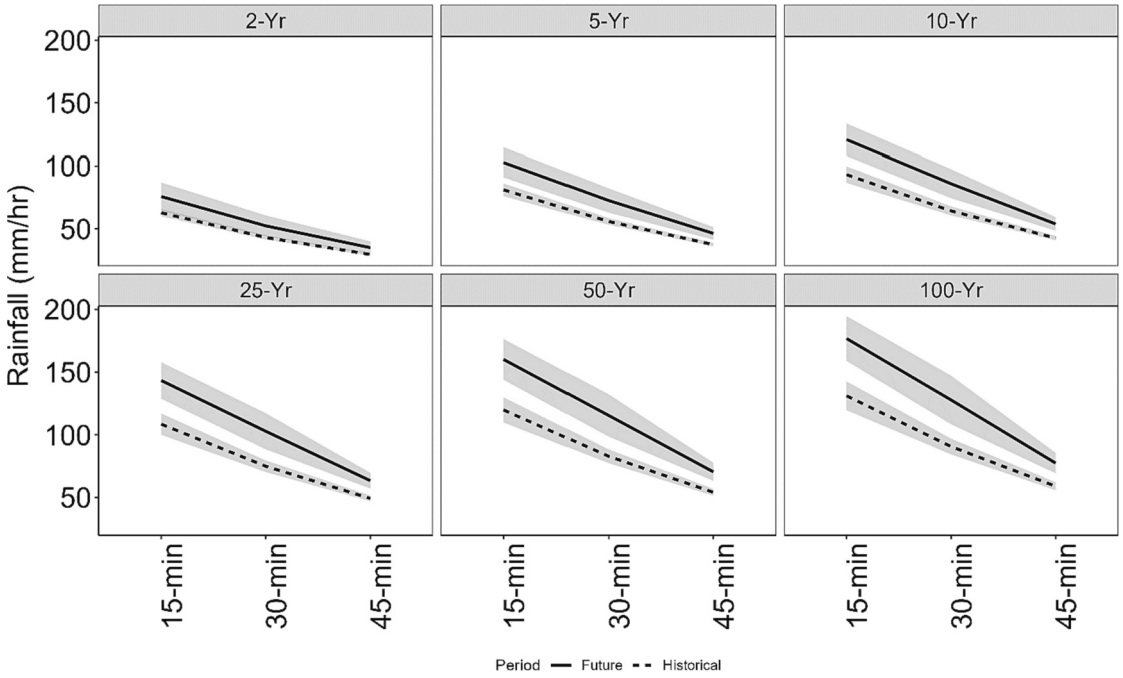

Fig. 7. Ensemble IDF curves with 95% confidence interval for historical and future projected located at Unicoi State Park under the RCP8.5 scenario with 2-, 5-, 10-, 25-, 50-, and 100-year return periods using ANN.

Table 3
Comparison of relative change (in %) in annual maximum of rainfall between future projected and historical rainfall IDF curves using ANN.

Station	Dur	Return period (years)					
		2	5	10	25	50	100
Huntsville 1 SSW	15-min	12	16	19	21	22	23
	30-min	7	9	9	10	10	11
	45-min	9	14	17	19	21	22
Venice	15-min	11	12	13	14	15	15
	30-min	12	15	16	17	18	19
	45-min	16	18	18	19	19	20
Unicoi State Park	15-min	18	22	23	25	26	27
	30-min	18	23	25	27	28	29
	45-min	16	19	20	22	23	23
New Orleans Audbon	15-min	8	14	18	22	24	26
	30-min	10	18	22	26	28	31
	45-min	12	22	27	31	34	36
Mullins	15-min	10	10	10	11	11	11
	30-min	19	21	21	22	23	23
	45-min	19	21	22	23	23	24

respectively. Among all of the models, the minimum and maximum standard deviation were 7 mm/h and 28 mm/h under GFDL and CAN-ESM, respectively.

The variability in rainfall IDF curves among different climate models is due to the different boundary conditions used for precipitation generation. For instance, the annual maximum of 1-day rainfall (RX1day) varies with each climate model. Supari et al. (2020) found that a climate model shows greater rainfall as much as five times for the same location than the remaining models. One of the main reasons is the inability of the model to represent topography, vegetation, and atmospheric conditions (Vizy and Cook, 2012), although, extreme rainfalls could be represented with a finer resolution of climate models (Kitoh and Endo, 2016). Moreover, the projected rainfall characteristics may not always be similar to that of observed rainfall datasets.

Therefore, Giorgi et al. (2013), Mirhosseini et al. (2013), Supari et al. (2020), and Zhao et al. (2021) recommended using multiple climate models for hydrological applications. Moreover, the superior performance of the ANN over the stochastic model has resulted in reliable IDF curves. This has also been found in various previous studies (Burian et al., 2001; Dibike and Coulibaly, 2006; Mirhosseini et al., 2014; Zhao et al., 2021). Burian and Durrans (2002) found the ANN to be a viable option for disaggregating hourly to sub-hourly rainfalls. On the other hand, despite choosing a particular disaggregating method, we found that most of the climate models show an increasing extreme rainfall depth over the Southeast United States.

4. Conclusions

We developed future projected rainfall IDF curves using a monthly maximum rainfall sub-hour (15-, 30-, and 45-min) scale of rainfall with a return period of 2-, 5-, 10-, 25-, 50-, and 100-year. These maximum values were obtained by developing 561 ANN models for the Southeast United States. This study confirms the satisfactory performance of the computationally-efficient feed-forward back-propagation ANN model in disaggregating monthly maximum rainfalls to sub-hourly scales from hourly scales. Moreover, the model also showed better performance than the stochastic model for generating sub-hour monthly maximum rainfall with an average NSE ranging from 0.67 to 0.84. The training and test results of the ANN models were evaluated with two statistical measures consisting of the coefficient of correlation and the root mean squared error which highlighted its satisfactory performance in disaggregating the monthly maximum rainfall depths. These results were further supported by the quantile-quantile plot and boxplots of NSE. The average NSE using the ANN model for 15-min is >0.6 indicating a satisfactory performance. In addition, we also found that there is a significantly better performance of the ANN over the stochastic model by rejecting the null hypothesis at a 5% significant level. The null hypothesis of better performance of stochastic approach than the ANN model in disaggregating hourly data to a monthly maximum of sub-hourly rainfall data is rejected (p-value$\sim$0) using a one-sided Student t-test and Wilcoxon sign rank test. These findings also showed that the ANN model is superior to the stochastic model in generating monthly maximum rainfall. These results are further improved with larger temporal scales of 30-min and 45-min. The KS test supports the assumption that the annual maximum rainfalls come from Gumbel extreme

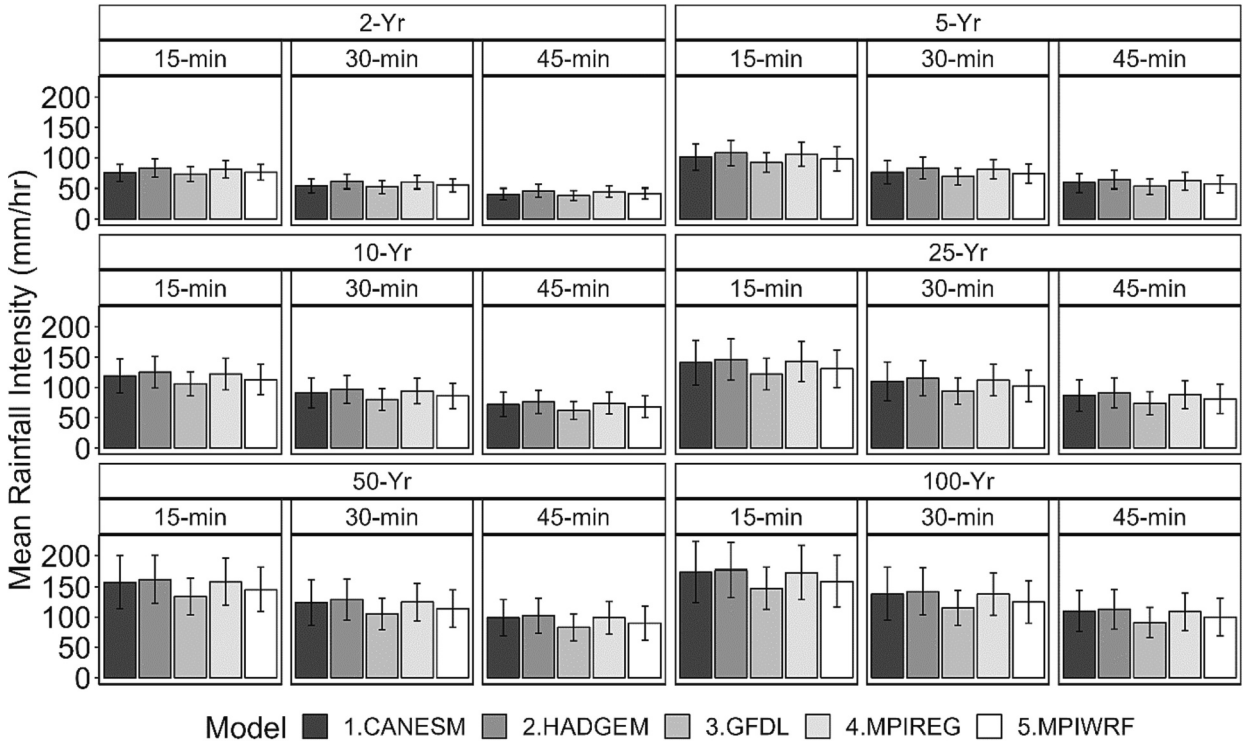

Fig. 8. Bar plots showing mean annual maximum rainfall intensity with ±1standard deviation of projected future rainfall IDF curves for five climate models with 2-, 5-, 10-, 25-, 50-, and 100-year return periods using ANN over southeastern United States.

distribution. A comparison of five selected locations showed that the estimated observed annual maximum rainfall intensities of 15-min and 30-min with a recurring interval of 2-, 5-, 10-, 25-, 50-, and 100-year are found to be closely related to reported rainfall values of NWS. The results show an increasing rate of future rainfall compared to the historical period by 7% to 36%. The mean projected future rainfall intensities over the southeast United States range from 34 to 135 mm/h for a duration of 15-, 30-, and 45-min with a return period of 2-, 5-, 10-, 25-, 50-, and 100-year. In addition, the standard deviation ranges from 7 to 28 mm/h between five climate models. The spatial variation of future projected extreme rainfall depths showed that the Gulf-Atlantic coast and the Appalachian Mountains are projected to receive more extreme rainfalls. This finding confirms the need to update future IDF curves which can better inform the design of water resource infrastructures.

CRediT authorship contribution statement

Bijoychandra S. Takhellambam: Conceptualization, Methodology, Formal analysis, Data curation, Writing – original draft, Visualization. **Puneet Srivastava:** Conceptualization, Methodology, Funding acquisition, Writing – review & editing, Supervision. **Jasmeet Lamba:** Conceptualization, Methodology, Funding acquisition, Writing – review & editing, Supervision. **Wenpeng Zhao:** Methodology, Writing – original draft, Writing – review & editing. **Hemendra Kumar:** Conceptualization, Methodology. **Di Tian:** Writing – review & editing, Data curation. **Roberto Molinari:** Conceptualization, Formal analysis, Writing – review & editing.

Declaration of Competing Interest

The authors declare that they have no known competing financial interests or personal relationships that could have appeared to influence the work reported in this paper.

Data availability

Data will be made available on request.

Acknowledgments

This work was completed in part with resources provided by the Auburn University Hopper Cluster. We are grateful for the support of the USDA-NIFA Hatch Project (ALA014-1-19052), and the Alabama Agricultural Experiment Station for this study.

Appendix A. Supplementary data

Supplementary data to this article can be found online at https://doi.org/10.1016/j.atmosres.2023.107122.

References

Amatya, D.M., Tian, S., Marion, D.A., Caldwell, P., Laseter, S., Youssef, M.A., Grace, J.M., Chescheir, G.M., Panda, S., Ouyang, Y., Sun, G., Vose, J.M., 2021. Estimates of precipitation IDF curves and design discharges for road-crossing drainage structures: case study in four small forested watersheds in the Southeastern US. J. Hydrol. Eng. 26, 05021004. https://doi.org/10.1061/(ASCE)HE.1943-5584.0002052.

Brownlee, J., 2019. A gentle introduction to the rectified linear unit (ReLU). In: Mach. Learn. Mastery. p. 6. https://machinelearningmastery.com/rectified-linear-activation-function-for-deep-learning-neural-networks/ [accessed 1 June 2023].

Budhathoki, S., Lamba, J., Srivastava, P., Williams, C., Arriaga, F., Karthikeyan, K.G., 2022. Impact of land use and tillage practice on soil macropore characteristics inferred from X-ray computed tomography. Catena 210, 105886. https://doi.org/10.1016/j.catena.2021.105886.

Burian, S.J., Durrans, S.R., 2002. Evaluation of an artificial neural network rainfall disaggregation model. Water Sci. Technol. 45, 99–104. https://doi.org/10.2166/wst.2002.0033.

Burian, S.J., Durrans, S.R., Nix, S.J., Pitt, R.E., 2001. Training artificial neural networks to perform rainfall disaggregation. J. Hydrol. Eng. 6, 43–51. https://doi.org/10.1061/(ASCE)1084-0699(2001)6:1(43).

Cannon, A.J., Sobie, S.R., Murdock, T.Q., 2015. Bias correction of GCM precipitation by quantile mapping: how well do methods preserve changes in quantiles and extremes? J. Clim. 28, 6938–6959. https://doi.org/10.1175/JCLI-D-14-00754.1.

Cheng, L., AghaKouchak, A., 2014. Nonstationary precipitation intensity-duration-frequency curves for infrastructure design in a Changing climate. Sci. Rep. 4, 7093. https://doi.org/10.1038/srep07093.
Coles, S., 2001. *An introduction to statistical modeling of extreme values*. Springer London. https://doi.org/10.1007/978-1-4471-3675-0.
Crévolin, V., Hassanzadeh, E., Bourdeau-Goulet, S.-C., 2023. Updating the intensity-duration-frequency curves in major Canadian cities under changing climate using CMIP5 and CMIP6 model projections. Sustain. Cities Soc. 92, 104473 https://doi.org/10.1016/j.scs.2023.104473.
Delignette-Muller, M.L., Dutang, C., 2015. fitdistrplus: an R package for fitting distributions. J. Stat. Softw. 64, 1–34. https://doi.org/10.18637/jss.v064.i04.
Dibike, Y.B., Coulibaly, P., 2006. Temporal neural networks for downscaling climate variability and extremes. Neural Netw. 19, 135–144. https://doi.org/10.1016/j.neunet.2006.01.003.
Easterling, D.R., Arnold, J.R., Knutson, T., Kunkel, K.E., LeGrande, A.N., Leung, L.R., Vose, R.S., Waliser, D.E., Wehner, M.F., 2017. Ch. 7: precipitation change in the United States. In: Climate Science Special Report: Fourth National Climate Assessment, Volume I. U.S. Global Change Research Program. https://doi.org/10.7930/J0H993CC.
Ganguli, P., Coulibaly, P., 2019. Assessment of future changes in intensity-duration-frequency curves for Southern Ontario using North American (NA)-CORDEX models with nonstationary methods. J. Hydrol. Reg. Stud. 22, 100587 https://doi.org/10.1016/j.ejrh.2018.12.007.
Ghasemi Tousi, E., O'Brien, W., Doulabian, S., Shadmehri Toosi, A., 2021. Climate changes impact on stormwater infrastructure design in Tucson Arizona. Sustain. Cities Soc. 72, 103014 https://doi.org/10.1016/j.scs.2021.103014.
Giorgi, F., Anyah, R.O., 2012. The road towards RegCM4. Clim. Res. 52, 3–6. https://doi.org/10.3354/cr01089.
Giorgi, F., Elguindi, N., Cozzini, S., Giuliani, G., 2013. Regional Climatic Model RegCM User's Guide Version 4.4.
Ingram, K., Dow, K., Carter, L., Anderson, J., 2013. Climate of the Southeast United States: Variability, Change, Impacts, and Vulnerability. Island Press, Washington DC. https://doi.org/10.5822/978-1-61091-509-0.
IPCC, 2018. Global Warming of 1.5°C: An IPCC Special Report on the Impacts of Global Warming of 1.5°C above Pre-Industrial Levels and Related Global Greenhouse Gas Emission Pathways, in the Context of Strengthening the Global Response to the Threat of Climate Change, Sustainable Development, and Efforts to Eradicate Poverty. Cambridge University Press, Cambridge, UK and New York, NY, USA. https://doi.org/10.1017/9781009157940.
Kim, J., Han, H., Kim, B., Chen, H., Lee, J.-H., 2020. Use of a high-resolution-satellite-based precipitation product in mapping continental-scale rainfall erosivity: a case study of the United States. Catena 193, 104602. https://doi.org/10.1016/j.catena.2020.104602.
Kitoh, A., Endo, H., 2016. Future changes in rainfall extremes associated with El Niño projected by a global 20-km mesh atmospheric model. Sola 12A, 1–6. https://doi.org/10.2151/sola.12A-001.
Kumar, H., Srivastava, P., Ortiz, B.V., Morata, G., Takhellambam, B.S., Lamba, J., Bondesan, L., 2021. Field-scale spatial and temporal soil water variability in irrigated croplands. Trans. ASABE 64, 1277–1294. https://doi.org/10.13031/trans.14335.
Kumar, H., Srivastava, P., Lamba, J., Diamantopoulos, E., Ortiz, B., Morata, G., Takhellambam, B., Bondesan, L., 2022a. Site-specific irrigation scheduling using one-layer soil hydraulic properties and inverse modeling. Agric. Water Manag. 273, 107877 https://doi.org/10.1016/j.agwat.2022.107877.
Kumar, H., Srivastava, P., Lamba, J., Ortiz, B.V., Way, T.R., Sangha, L., Takhellambam, B.S., Morata, G., Molinari, R., 2022b. Within-field variability in nutrients for site-specific agricultural management in irrigated cornfield. J. ASABE 65, 865–880. https://doi.org/10.13031/ja.15042.
Kumar, H., Srivastava, P., Lamba, J., Lena, B., Diamantopoulos, E., Ortiz, B., Takhellambam, B., Morata, G., Bondesan, L., 2023. A methodology to optimize site-specific field capacity and irrigation thresholds. Agric. Water Manag. 286, 108385 https://doi.org/10.1016/j.agwat.2023.108385.
Kunkel, K.E., Stevens, L.E., Stevens, S.E., Sun, L., Janssen, E., Wuebbles, D., Ii, C.E.K., Fuhrman, C.M., Keim, B.D., Kruk, M.C., Billet, A., Needham, H., Schafer, M., Dobson, J.G., 2013. Regional Climate Trends and Scenarios for the U.S. National Climate Assessment (No. NESDIS 142-2). National Oceanic and Atmospheric Administration, National Oceanic and Atmospheric Administration.
Lilliefors, H.W., 1967. On the Kolmogorov-Smirnov test for normality with mean and variance unknown. J. Am. Stat. Assoc. 62, 399–402. https://doi.org/10.2307/2283970.
Mahdi, S., Cenac, M., 2005. Estimating parameters of Gumbel distribution using the methods of moments, probability weighted moments and maximum likelihood. Rev. Matemática Teoría Apl. 12, 151–156. https://doi.org/10.15517/rmta.v12i1-2.259.
McGehee, R., Srivastava, P., 2018. Benchmarking reliable erosion indices from quarter-hour station data for climate studies in the southeastern United States. J. Soil Water Conserv. 73, 363–376. https://doi.org/10.2489/jswc.73.4.363.
McGehee, R.P., Flanagan, D.C., Srivastava, P., Engel, B.A., Huang, C.-H., Nearing, M.A., 2021. An updated isoerodent map of the conterminous United States. Int. Soil Water Conserv. Res. https://doi.org/10.1016/j.iswcr.2021.06.004.
Mearns, L., McGinnis, S., Korytina, D., Arritt, R., Biner, S., Bukovsky, M., Chang, H.-I., Christensen, O., Herzmann, D., Jiao, Y., Kharin, S., Lazare, M., Nikulin, G., Qian, M., Scinocca, J., Winger, K., Castro, C., Frigon, A., Gutowski, W., 2017. The NA-CORDEX Dataset. https://doi.org/10.5065/D6SJ1JCH.
Mirhosseini, G., Srivastava, P., Stefanova, L., 2013. The impact of climate change on rainfall intensity–duration–frequency (IDF) curves in Alabama. Reg. Environ. Chang. 13, 25–33. https://doi.org/10.1007/s10113-012-0375-5.
Mirhosseini, G., Srivastava, P., Fang, X., 2014. Developing rainfall intensity-duration-frequency curves for Alabama under future climate scenarios using artificial neural networks. J. Hydrol. Eng. 19, 04014022. https://doi.org/10.1061/(ASCE)HE.1943-5584.0000962.
Nerantzaki, S.D., Papalexiou, S.M., 2022. Assessing extremes in hydroclimatology: a review on probabilistic methods. J. Hydrol. 605, 127302 https://doi.org/10.1016/j.jhydrol.2021.127302.
NOAA NCEI (National Oceanic and Atmospheric Administration, National Centers for Environmental Information), 2014. US 15 Minute Precipitation Data, Version 1.0. 1970–2010.
Noor, M., Ismail, T., Shahid, S., Asaduzzaman, Md., Dewan, A., 2022. Projection of rainfall intensity-duration-frequency curves at ungauged location under climate change scenarios. Sustain. Cities Soc. 83, 103951 https://doi.org/10.1016/j.scs.2022.103951.
Op de Hipt, F., Diekkrüger, B., Steup, G., Yira, Y., Hoffmann, T., Rode, M., 2018. Modeling the impact of climate change on water resources and soil erosion in a tropical catchment in Burkina Faso, West Africa. Catena 163, 63–77. https://doi.org/10.1016/j.catena.2017.11.023.
Perica, S., Martin, D., Pavlovic, S., Roy, I., St Laurent, M., Trypaluk, C., Unruh, D., Yekta, M., Bonnin, G., 2013. Precipitation-Frequency Atlas of the United States (No. Volume 9 Version 2.0: Southeastern States (Alabama, Arkansas, Florida, Georgia, Louisiana, Mississippi)). NOAA, National Weather Service, Silver Spring, MD.
Phien, H.N., 1987. A review of methods of parameter estimation for the extreme value type-1 distribution. J. Hydrol. 90, 251–268. https://doi.org/10.1016/0022-1694(87)90070-9.
Ragno, E., AghaKouchak, A., Love, C.A., Cheng, L., Vahedifard, F., Lima, C.H., 2018. Quantifying changes in future intensity-duration-frequency curves using multimodel ensemble simulations. Water Resources Research 54 (3), 1751–1764. https://doi.org/10.1002/2017WR021975.
Rahaman, M.H., Saha, T.K., Masroor, M., Roshani, Sajjad, H., 2023. Trend analysis and forecasting of meteorological variables in the lower Thoubal river watershed, India using non-parametrical approach and machine learning models. Model. Earth Syst. Environ. https://doi.org/10.1007/s40808-023-01799-y.
Scinocca, J.F., Kharin, V.V., Jiao, Y., Qian, M.W., Lazare, M., Solheim, L., Flato, G.M., Biner, S., Desgagne, M., Dugas, B., 2016. Coordinated global and regional climate modeling. J. Clim. 29, 17–35. https://doi.org/10.1175/JCLI-D-15-0161.1.
Skamarock, W., Klemp, J., Dudhia, J., Gill, D., Barker, D., Wang, W., 2005. A Description of the Advanced Research WRF Version 2. UCAR/NCAR. https://doi.org/10.5065/D6DZ069T.
Socolofsky, S., Adams, E.E., Entekhabi, D., 2001. Disaggregation of daily rainfall for continuous watershed modeling. J. Hydrol. Eng. 6, 300–309. https://doi.org/10.1061/(ASCE)1084-0699(2001)6:4(300).
Soltani, S., Almasi, P., Helfi, R., Modarres, R., Mohit Esfahani, P., Ghadami Dehno, M., 2020. A new approach to explore climate change impact on rainfall intensity–duration–frequency curves. Theor. Appl. Climatol. 142, 911–928. https://doi.org/10.1007/s00704-020-03309-x.
Sun, Y., Wendi, D., Kim, D.E., Liong, S.-Y., 2019. Deriving intensity–duration–frequency (IDF) curves using downscaled in situ rainfall assimilated with remote sensing data. Geosci. Lett. 6, 17. https://doi.org/10.1186/s40562-019-0147-x.
Supari, Tangang, F., Juneng, L., Cruz, F., Chung, J.X., Ngai, S.T., Salimun, E., Mohd, M.S. F., Santisirisomboon, J., Singhruck, P., PhanVan, T., Ngo-Duc, T., Narisma, G., Aldrian, E., Gunawan, D., Sopaheluwakan, A., 2020. Multi-model projections of precipitation extremes in Southeast Asia based on CORDEX-Southeast Asia simulations. Environ. Res. 184, 109350 https://doi.org/10.1016/j.envres.2020.109350.
Takhellambam, B.S.. *Climate Change Implications on Rainfall Erosivity and Intensity Duration Frequency Curves over the Southeast United States* [Auburn University]. https://etd.auburn.edu//handle/10415/8923.
Takhellambam, B.S., Srivastava, P., Lamba, J., McGehee, R.P., Kumar, H., Tian, D., 2022a. Temporal disaggregation of hourly precipitation under changing climate over the Southeast United States. Sci. Data 9, 211. https://doi.org/10.1038/s41597-022-01304-7.
Takhellambam, B.S., Srivastava, P., Lamba, J., McGehee, R.P., Kumar, H., Tian, D., 2022b. Projected rainfall erosivity under climate change in the Southeastern United States. In: ASABE Paper No. 2200176. Presented at the 2022 ASABE Annual International Meeting. ASABE, St. Joseph, MI, p. 1. https://doi.org/10.13031/aim.202200176.
Takhellambam, B.S., Srivastava, P., Lamba, J., McGehee, R.P., Kumar, H., Tian, D., 2023. Projected mid-century rainfall erosivity under climate change over the southeastern United States. Sci. Total Environ. 865, 161119 https://doi.org/10.1016/j.scitotenv.2022.161119.
Trenberth, K.E., 2011. Changes in precipitation with climate change. Clim. Res. 47, 123–138. https://doi.org/10.3354/cr00953.
Vizy, E.K., Cook, K.H., 2012. Mid-twenty-first-century changes in extreme events over Northern and tropical Africa. J. Clim. 25, 5748–5767. https://doi.org/10.1175/JCLI-D-11-00693.1.
Yan, H., Sun, N., Wigmosta, M., Skaggs, R., Hou, Z., Leung, R., 2018. Next-generation intensity-duration-frequency curves for hydrologic design in snow-dominated environments. Water Resour. Res. 54, 1093–1108. https://doi.org/10.1002/2017WR021290.
Zhao, W., Kinouchi, T., Nguyen, H.Q., 2021. A framework for projecting future intensity-duration-frequency (IDF) curves based on CORDEX Southeast Asia multi-model simulations: an application for two cities in Southern Vietnam. J. Hydrol. 598, 126461 https://doi.org/10.1016/j.jhydrol.2021.126461.
Zhao, W., Abhishek, Kinouchi, T., 2022a. Uncertainty quantification in intensity-duration-frequency curves under climate change: implications for flood-prone

tropical cities. Atmos. Res. 270, 106070 https://doi.org/10.1016/j.atmosres.2022.106070.

Zhao, W., Abhishek, Kinouchi, T., Ang, R., Zhuang, Q., 2022b. A framework for quantifying climate-informed heavy rainfall change: implications for adaptation strategies. Sci. Total Environ. 835, 155553 https://doi.org/10.1016/j.scitotenv.2022.155553.

Zhao, W., Abhishek, Takhellambam, B.S., Zhang, J., Zhao, Y., Kinouchi, T., 2023. Spatiotemporal variability of current and future sub-daily rainfall in Japan using state-of-the-art high-quality data sets. Water Resour. Res. 59 https://doi.org/10.1029/2022WR034305 e2022WR034305.